Iterative Color Equalization for Increased Applicability of Structured Light Reconstruction

Torben Fetzer[1], Gerd Reis[2] and Didier Stricker[1,2]

[1]*Department of Computer Science, University of Kaiserslautern, Germany*
[2]*Department Augmented Vision, DFKI GmbH, Germany*

Keywords: Structured Light, 3D-Reconstruction, Color Equalization, Photometric Compensation.

Abstract: The field of 3D reconstruction is one of the most important areas in computer vision. It is not only of theoretical importance, but is also increasingly used in practice, be it in reverse engineering, quality control or robotics. A distinction is made between active and passive methods, depending on whether they are based on active interactions with the object or not. Due to the accuracy and density of the reconstructions obtained, the structured light approach, whenever applicable, is often the method of choice for industrial applications. Nevertheless, it is an active approach which, depending on material properties or coloration, can lead to problems and fail in certain situations. In this paper, a method based on the standard structured light approach is presented that significantly reduces the influence of the color of a scanned object. It improves the results obtained by repeated application in terms of accuracy, robustness and general applicability. Especially in high-precision reconstruction of small structures or high-contrast colored and specular objects, the technique shows its greatest potential. The advanced method requires neither pre-calibrated cameras or projectors nor information about the equipment. It is easy to implement and can be applied to any existing scanning setup.

1 INTRODUCTION

Modern structured light systems typically consist of a projector that illuminates the scene through several fringe patterns and at least one camera that captures the lit scene. There are several techniques based on binary patterns, pseudo-random patterns, and finally phase-shifted structured light known as state of the art. The calculation of phase images for each camera from the patterns projected ensures continuous surface encoding. This allows dense correspondence to be determined between all views, including the projector. Based on the resulting high-quality correspondences, modern auto-calibration techniques ((Zhang, 1998), (Fetzer et al., 2019), (Lourakis and Deriche, 2000), (Hartley and Zisserman, 2003)) ensure that camera matrices can be estimated robustly, ready for triangulation of point clouds. In this way, a calibration of the devices is generated that achieves highest accuracy on the object's surface. This in turn leads to high-precision reconstructions and is a superiority of this method over other scanning techniques.

In addition to the strengths of structured light, there is a number of disadvantages that should by no means be neglected. The basis of the process is the visibility of the projections on the object's surface. In this context, transparent, mirroring and specular scenes should be mentioned above all. Even objects whose texture contains both highly absorbent and highly reflective areas can cause problems. In many cases such scenes lead to inaccuracies and often to a complete failure of the method. With this work we want to eliminate or at least reduce some of these problems in a way that can be easily adopted to existing scan setups. We significantly increase the application area of structured light reconstruction without additional hardware requirements.

According to the state of the art, shifted sinusoidal fringe patterns are used which sum up to zero. Therefore, the encoding method should be invariant to the object's texturing. The following reflection properties are unfortunately neglected in this idealized model:

- Different materials cause different light reflection.
- Different colors reflect the light in different ways.

Therefore, in many cases the appearance of the projected fringe patterns can change into the impercep-
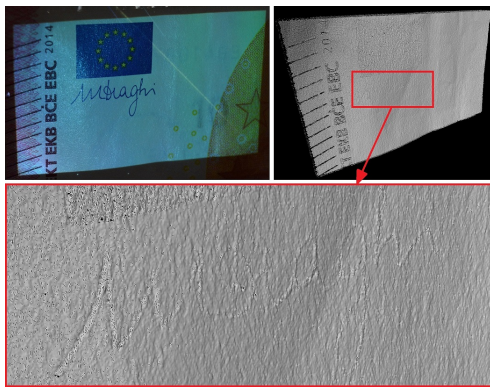
725

Figure 1: Recorded section of a 10-euro note (top left) and corresponding point cloud, reconstructed by structured light (top right). The enlarged area (below) shows errors in the estimated depth, solely caused by the object's coloration.

tible. Most reconstructions of objects made of standard material are not very strongly affected and time-consuming procedures, to always treat this behavior, would certainly be overdone. Nevertheless, this effect is clearly noticeable in high-precision reconstructions and it is worth taking a closer look. To illustrate this, Figure 1 shows a captured area of a 10-euro note and a point cloud thereof reconstructed with structured light. The enlargement of the point cloud clearly shows the erroneous depth caused exclusively by the texturing of the object. The combination of the projection patterns with an inverse texture significantly reduces this effect.

2 RELATED WORK

Modern phase-shifted structured light systems with digital devices were introduced in (Zhang and Huang, 2004). In order to shorten the acquisition time, (Zhang and Huang, 2006) and before (Zhang et al., 2002) introduced methods that use color-coded patterns. (Sansoni and Redaelli, 2005) and later (Yang et al., 2017) introduced single shot structured light techniques, where the multiple shifted fringe images were coded by carrier waves and combined to one pattern. (Donlic et al., 2015) and (Petković et al., 2016) presented single-shot structured light approaches, based on de bruijn color sequences. All methods to shorten the acquisition time reduced the quality of reconstructions significantly. In (Zhang and Yau, 2008) a setup with two cameras is presented to significantly increase the scan quality. When using several cameras (ideally the same camera model) there are many advantages with regard to calibration, gamma correction of the recorded scenes and the resulting quality of the reconstructions. Although, the

approach based on this technique has become state of the art in many areas, there are several scenarios, where this approach is not applicable.

Extensive research has been carried out to improve the applicability to general situations. In order to cope with strong ambient lighting such as sunlight, (Gupta et al., 2013) introduced a possibility of compensation by sequentially allocating a given energy budget to several sections. (Nayar et al., 2006) and later (O'Toole et al., 2014), (O'Toole et al., 2012) presented ways to split direct and indirect light paths, enabling the reconstruction of mirroring, reflecting and light emitting objects and even scanning through dust. Unfortunately, this requires expensive hardware, the process is error-prone and requires high-precision calibration of camera pixels to a DLP panel, making it difficult to use for practical applications. (Weinmann et al., 2011) increased the range of application of structured light but using additional devices.

3 INVERSE TEXTURE

First of all, we want to investigate the influence of a projection to the captured image of a scene. We then present a procedure that modulates the projection in such a way that as many points as possible in the scene have an equivalent influence to the captured image. This procedure equalizes the appearance of an object iteratively and converges after only a few steps. The projector-camera correspondences are generated using the structured light approach and are reliably cleaned of erroneous phases with the help of a newly introduced simple masking method.

Let I be a captured image of a scene that was illuminated by a projection T. Schreiber and Bruning (Malacara, 2007) described the physical influence of T on image I. Accordingly, the captured image can be approximated as the composition

$$I = I' + I'' \circ T, \qquad (1)$$

of the average intensity I' and the scene intensity I'', moduled by the projected texture T. Thereby, $\circ$ denotes the element-wise multiplication operator.

In order to minimize the influence of the coloring of an object to its image, projection texture T has to be estimated so that it balances the object colors as much as possible. Therefore, the following minimization problem has to be solved:

$$\operatorname*{argmin}_{T,\bar{I}} \sum_{ij}(I_{ij} - \bar{I})^2 = \operatorname*{argmin}_{T,\bar{I}} \sum_{ij}(I'_{ij} + I''_{ij}T_{ij} - \bar{I})^2 \quad (2)$$

While I_{ij} denotes the pixels of image I and $\bar{I}$ the optimal common color value of the equalized pixels.

(a) Camera-Projector Correspondences   (b) Masking Erroneous Phase   (c) Inverse Texture Projection
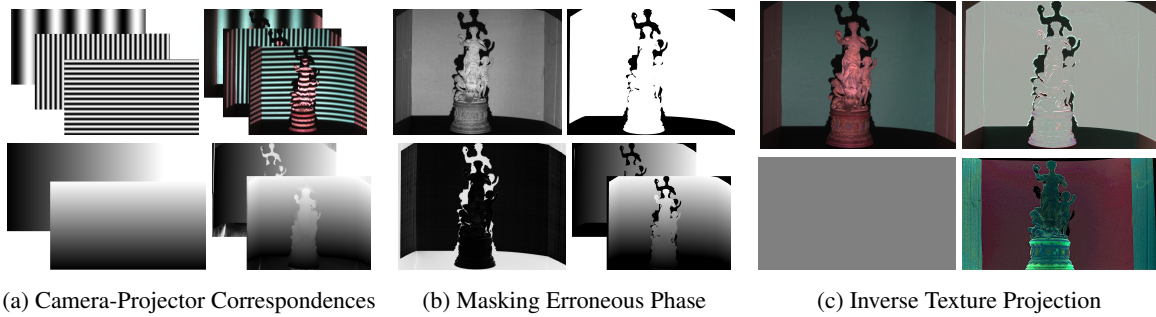
Figure 2: Examples of sinusoidal fringe patterns and thus illuminated scenes captured by a camera (a, top). Horizontal and vertical phases of the projector and the camera calculated from the fringe images (a, bottom). Texture image calculated from averaging captures (4) and error image calculated from (9) (b, left). Projection mask clustered from error image and correspondingly masked phase images (b, right). Textures T projected onto an exemplary scene: Gray projection and inverse texture calculated with Algorithm 1 (c, bottom). Correspondingly captured scene without and with color correction (c, top).

Projecting T on the scene approximates an uncolored grayish scene as visualized in Figure 2 (c).

Theoretically, an optimal texture T solution (2) can be calculated explicitly from at least two captured images. However, this is not recommended from a practical point of view. This is due to the following phenomena, which cannot be considered in the underlying model (1):

- Color cross-talk between the different color channels of projector and camera.

- Scattered light from one pixel to others are not considered, since it only takes into account direct pixel to pixel correspondences.

- Specular or absorbing materials, leading to clipped values in the captured image, due to a limited dynamic range.

3.1 Iterative Color Equalization

To solve problem (2), we propose an iterative method that is robust against the irregularities listed above. We combine alternate updates of the projected texture T and the equalized target value $\bar{I}$ with a logarithmic search that uses the limited range of projector pixel values (8-bit in[0,255]). In this way, a stable convergence of the process is achieved after a few iterations.

Logarithmic Search. We assume that we have direct correspondences between camera and projector pixels that are given by a mapping $\mathcal{P}: (x_I, y_I) \rightarrow (x_P, y_P)$ that assigns a corresponding projector pixel (x_P, y_P) to each image pixel (x_I, y_I). Therewith, any projection pixel T_{ij} in the captured scene is known to be located at $\mathcal{P}(T_{ij})$ in the projector input image. Since these are usually limited to 8-bit color values in three color channels, we have a discrete search range for texture values of T that can

be effectively used by a binary search. Moreover, projecting light is a monotonous procedure, therefore increasing values of T_{ij} lead to increasing values of I_{ij}. In order to implement and exploit this knowledge, the values of the projection $\mathcal{P}(T)$ are adjusted via a logarithmic search until the error (2) of the resulting image $I = I' + I'' \circ T$ to the equalization value $\bar{I}$ for all pixels is minimal.

Equalization Value. Minimizing energy (2) with a fixed texture T leads to an optimal equalization value

$$\bar{I} = \frac{1}{MN} \sum_{ij} I_{ij} \qquad (3)$$

given by the mean of image $I_{M \times N}$.

Alternating updates of the inverse texture T and the equalization value $\bar{I}$ with adjusted increments lead to Algorithm 1, which already converges after 7 iterations in case of standard 8-bit projective devices. Since the texture update is pixel-wise independent, the individual iterations can be implemented efficiently. Figure 2 (c) shows a scene balanced in this way. Each iteration was applied separately to the different color channels to intercept the color cross-talk.

3.2 Camera-projector Correspondences

In order to apply Algorithm 1, a reliable mapping $\mathcal{P}(\cdot)$ as described in Section 3.1 is required. A recommended approach for determining close point correspondences between projector image and camera image is the structured light approach introduced in (Zhang and Huang, 2004). The projection of phase-shifted sine waves (Figure 2, (a), top) allows the calculation of phase images encoding the scene through the projection (Figure 2, (a), bottom). This usually requires phase unwrapping methods like (Bioucas-Dias

and Valadao, 2007) or (An et al., 2016) to encode generated wrapped phases. The phase information can be used to determine point correspondences of projector and camera pixels. Errors in the underlying phase information can be caused by

- Overexposed or underexposed areas in the scene where the projected fringes are not visible.

- Regions in the scene that are visible to the camera but not to the projector.

- Shadows cast by the illuminated object.

Masking Erroneous Phase Values. For the success of the proposed color equalization method it is a prerequisite to have an accurate mapping $\mathcal{P}$ available. No false correspondences should be used that would significantly falsify the result. For this purpose, incorrect phase information should be masked out beforehand. Defective phase regions, which are calculated using standard phase shift approaches (Malacara, 2007), are usually much more noisy than correctly coded ones. Therefore, gradient based filters are typically used to mask out erroneous regions. However, these approaches are not sufficiently accurate for the presented application. Due to the gradient dependency, edges are falsely masked out, which runs counter to the later goal of reconstructing highly accurate small structures. In order to create an appropriate masking, a simple method is presented that provides much more accurate results. Given is the basic property of phase-shifted sinusoidal patterns:

$$\frac{1}{N} \sum_{n=1}^{N} I_n^H = \frac{1}{M} \sum_{m=1}^{M} I_m^V = I' + 0.5 I''. \quad (4)$$

The sum of the phase-shifted sine waves results in zero, which neglects their influence. This means that the applied illumination of the scene in sum is equivalent to a uniform grey projection. Let I_n^H and I_n^V denote the captured scenes, illuminated by respective sine patterns P_n^H and P_m^V, defined by

$$P_n^H(i,j) = \sin\left(\frac{2\pi j}{w} F_H + \frac{2\pi(n-1)}{N}\right) \quad (5)$$

$$P_m^V(i,j) = \sin\left(\frac{2\pi i}{h} F_V + \frac{2\pi(m-1)}{M}\right) \quad (6)$$

$$i = 1, ..., h, \; j = 1, ..., w, \; n = 1, ..., N, \; m = 1, ..., M$$

with F_H and F_V being the number of horizontal and vertical fringes over the projection and w and h the projector's image width and height in pixels.

If the scene was captured without illumination, I' is already given and so I'' can be estimated by

$$I'' = \frac{1}{N} \sum_{n=1}^{N} I_n^H + \frac{1}{M} \sum_{m=1}^{M} I_m^V - 2I'. \quad (7)$$

Finally, we can calculate an error E of the horizontal and vertical phase values Φ_H and Φ_V to the captured images I_n^H and I_m^V by

$$E = \sum_{n=1}^{N} \left(\sin\left(\Phi_H F_H + \frac{2\pi(n-1)}{N}\right) - \frac{I_n^H - I'}{I''}\right)^2 \quad (8)$$

$$+ \sum_{m=1}^{M} \left(\sin\left(\Phi_V F_V + \frac{2\pi(m-1)}{M}\right) - \frac{I_m^V - I'}{I''}\right)^2.$$

Figure 2 (b, top left) shows an example of a texture computed from image means (4) and (b, bottom left) the respective error image E from (9). This error reliably indicates the quality of the phase values in relation to all captured images of the scene. Since erroneous phase values produce much higher errors than correct ones, a high-quality mask can be generated by applying *k-Means Clustering* to error image E. Note that bi-clustering can be efficiently implemented in $O(MN\log(MN))$. Figure 2 (b, top right) shows the final mask as a result of *k*-means clustering applied with two clusters. Figure 2 (b, bottom right) shows the final masked phases.

Algorithm 1: Iterative Color Equalization.

Input: Camera-projector correspondences $\mathcal{P}$.

1: Initialize projection texture $\mathcal{P}(T_{ij}^{(0)}) = 128 \; \forall ij$.

2: Project pattern $T_{ij}^{(0)}$ and capture lit scene $I^{(0)}$.
   for $z = 1, ..., 7$

3: $\quad \bar{I}^{(z-1)} = \frac{1}{MN} \sum_{ij} I_{ij}^{(z-1)}$

4: $\quad \mathcal{P}(T_{ij}^{(z)}) = \begin{cases} \mathcal{P}(T_{ij}^{(z-1)}) + 2^{7-z}, & I_{ij}^{(z-1)} < \bar{I}^{(z-1)} \\ \mathcal{P}(T_{ij}^{(z-1)}) - 2^{7-z}, & I_{ij}^{(z-1)} > \bar{I}^{(z-1)} \\ \mathcal{P}(T_{ij}), & \text{else} \end{cases}$

5: $\quad$ Project pattern $T^{(z)}$ and capture resulting scene $I^{(z)}$.
   end

Output: Inverse texture T.

---

4 INVERSELY TEXTURING STRUCTURED LIGHT (ITSL)

In order to neglect color influences on the geometry estimation by the structured light approach, we combine the inverse texture calculated by Algorithm 1 with the fringe images P_n^H and P_m^V from (5) and (6). Instead of the normal patterns we project the *Inversely Texturing Structured Light Patterns (ITSLP)*

$$T_n^H = P_n^H \circ \mathcal{P}(\tilde{T}), \quad n = 1, ..., N \quad (9)$$

$$T_m^V = P_m^V \circ \mathcal{P}(\tilde{T}), \quad m = 1, ..., M. \quad (10)$$

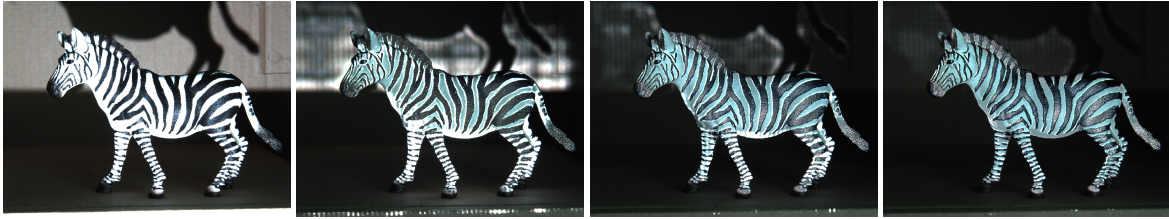We lift values of the inverse texture close to zero to avoid that no fringes are projected in these regions

Figure 3: Captured scene of a zebra to visualize the improvements of several iterations of ITSL to color equalization. Normal image (left) and equalized captures after one, two and three iterations (second left to right).

after multiplication:

$$\tilde{T}_{ij} = \begin{cases} T \cdot T_{ij} & \text{,if } T_{ij} > 0.05 \cdot \max(T) \\ 0.05 \cdot \max(T) & \text{,else} \end{cases} \quad (11)$$

In the process, masked areas are also coded after several iterations of the approach.

An important feature of ITSLP is that they fulfill the basic property for fringes of a structured light system, as mentioned in (4). In the new case we have for every scene

$$\frac{1}{N} \sum_{n=1}^{N} I_n^H = I' + \frac{1}{N} \sum_{n=1}^{N} \mathcal{P}^{-1}(P_n^H) \circ \tilde{T} \circ I'' \quad (12)$$

$$= I' + 0.5(\tilde{T} \circ I'') \approx I' + 0.5(T \circ I''). \quad (13)$$

This is equivalent to usual structured light patterns being projected onto a grey scene without color influence. Figure 4 (top left) shows ITSLP, computed by (11) and the patterns projected onto the scene (top right). For further visualization Figure 4 (bottom) shows the scenes after averaging (4) the standard structured light patterns (left) and ITSLP (right).

Each iteration of ITSLP increases the quality of the reconstructions. Regions with incorrect phase information of the first iteration can be corrected by multiple iterations of *ITSL*.
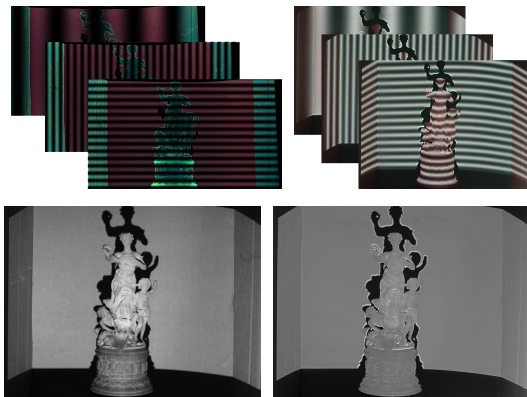

Figure 4: Examples of inversely texturing fringe images projected by the projector (top left) and illuminated scene (top right). Textures calculated by (7) from the fringe images (bottom).

5 EVALUATION

In order to evaluate the usefulness of the method presented, we carry out some quantitative and qualitative tests. First the performance of the color equalization from Algorithm 1 is examined. In particular, the behavior after several iterations of ITSL is investigated. Subsequently, we show the advantages and the important practical benefits of ITSLP to structured light reconstruction. In several scenarios, in which the standard structured light approach usually fails, the benefits, which arise from the new, improved approach, become clear.

5.1 Inverse Projection Texture

Figure 6 (left) shows a captured image of a standardized *X-Rite ColorChecker* normally used for color calibration. It consists of 24 calibrated colors that well cover the entire visual color spectrum. Figure 6 (right) shows the captured checkerboard after an iteration of Algorithm 1. The method applied to this object demonstrates its behavior in case of very large color differences in an object's texture. It is clearly visible that some color patches (dark red, yellow) cannot be equalized completely. The reason for this is that light can only be projected but not removed. If the red, green or blue component is already in an area above the mean value of the equalization, it cannot be reduced by any projection. To be exact, the gamut of the camera does not lie in the gamut generated by the projector. Nevertheless, equalization results of this quality lead to a significant improvement in the reflective properties of an object. Moreover, since grayscale images are sufficient for reconstruction, monochrome cameras can also be used. Errors that may occur during color equalization due to inconsistent gamuts are negligible in this case. Multiple iterations of ITSL, further improve the quality of equalization. Figure 6 shows the behavior of the Root-Mean-Squared-Error (RMSE), referred to the mean value (3), for an iterative application. While after the first iteration the RMSE decreases by more than 90%, the following it-
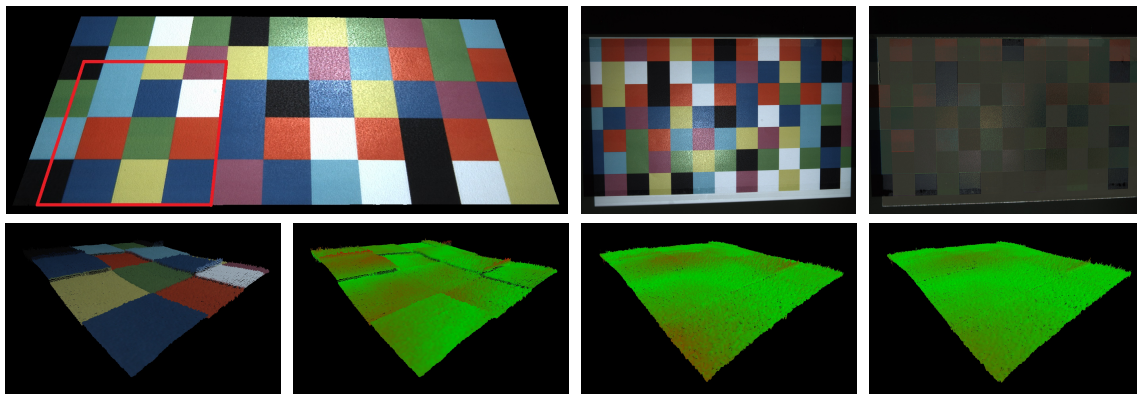
Figure 5: Flat colored checkerboard: Initial reconstructed point cloud (top left), normal texture (top middle) and equalized texture after one iteration of ITSL (top right). Enlarged marked area of point cloud (bottom left) and point clouds before and after two iterations of the proposed approach (bottom second left to right).

erations reduce this error only slightly in this case.

However, these minor changes can lead to a dramatic improvement of reconstructions. In particular, the reflection behaviour at edges of strongly contrasting areas can be significantly improved after a few iterations, due to lower radiation. For visual evaluation, Figure 3 shows several iterations of the method applied to a figurine of a zebra. The coloration of this object contains maximally strong edges in the transitions from black to white areas. Due to better approximated phase values, every iteration improves the equalization quality. Note that limited projector brightness and stray light between pixels are the reasons why it is impossible to achieve complete equalization in an extreme scenario like the one shown in Figure 3. But within the scope of the possibilities, the result obtained here is by far sufficient to yield significant improvements in reconstruction, as demonstrated later on.
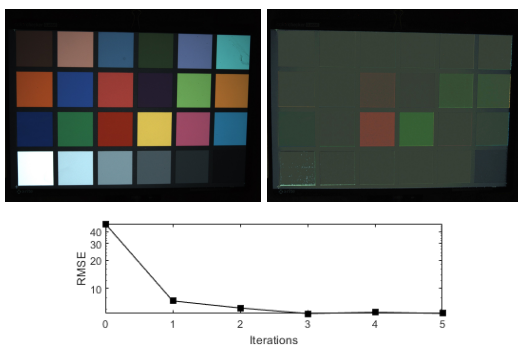

Figure 6: Captured image of a *X-Rite ColorChecker* before (top left) and after one iteration of color equalization with Algorithm 1 (top right). RMSE of color equalization for several iterations of ITSLP (bottom).

5.2 Inversely Texturing Structured Light

In order to demonstrate the advantages of the presented method in the context of 3D reconstruction, we will apply it in the following exemplary scenarios. We show quantitative and qualitative improvements in the important case of high-precision reconstruction of very small structures. We then apply it to objects with high-contrast staining, such as the one in Figure 3, and qualitatively investigate the behavior after several iterations of the method. Finally, the chances arising from the method in context of specular and reflecting objects are shown by an exemplary reconstruction of a shiny metal sphere.

5.2.1 High-precision Reconstruction

Different colors of an object's texture reflect different wavelengths of light. These specific properties, depending on the object coloration, cause projected patterns in structured light applications to be reflected in slightly different ways. Therefore, depending on the coloration of an object, slightly different depth values are estimated. Usually, this effect is very small, compared to the geometry of an object, and can therefore be neglected. However, in high-precision 3D reconstructions, as for example encountered in quality control setups, this problem has considerable effects and significantly distorts the results, especially in high-contrast regions.

In order to evaluate the usefulness of the procedure in relation to this problem, we apply it to a flat checkerboard with patches of different colors, as shown in Figure 5. The checkerboard is absolutely flat and any differences in the depth of the reconstruction are errors due to the different colors of the patches.
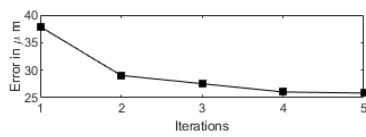
Figure 7: Average Euclidean depth error in *μm* of reconstructed point cloud for several iterations of ITSL.
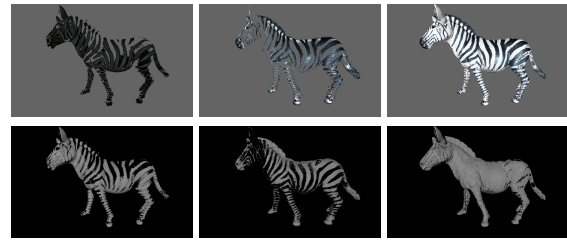

Figure 8: Reconstructed point clouds of a zebra statue. Top row and bottom row show the same point clouds with and without color information. Left and middle columns show results of standard structured light in case of over and underexposed images. Right shows ITSL handling the proposed problems.

Figure 5 (top left) shows the reconstructed point cloud resulting from the standard structured light approach. For further visualization, Figure 5 (top center, right) shows the captured scene before and after color equalization. To demonstrate the problem more clearly, Figure 5 (bottom left) shows an enlarged version of the marked area.

Figure 5 (bottom, second left) shows the point cloud of the enlarged region without texture information, but colored by the Euclidean error with respect to the flat ground truth. Finally, Figure 5 (bottom, second right and right) shows the reconstructed regions after one and two iterations of ITSL. To make a qualitative evaluation possible, the depth value of the checkerboards is enhanced by a factor of 3 for visualization. This clearly shows the improvements of the method presented.

Besides the qualitative evaluation, we demonstrate the benefit by a quantitative error measurement. Figure 7 shows the behavior of the average depth error of the reconstructed point with respect to the ground truth. Multiple iterations improve the quantitative error continuously. Nevertheless, since the improvements are in the range of *μm*, one should decide whether the improvement of accuracy of the reconstruction justifies higher additional expenses in the specific case.

5.2.2 High-contrast Colored Objects

Another important field of application of the method is the reconstruction of objects with extremely unfavourable colouring. The statue of a zebra from Figure 3 is treated as an example. Due to the very bright and very dark areas there is no camera setting that allows a complete encoding of the surface with structured light. Figure 8 (left) shows the result of standard structured light with a rather short exposure time. The white areas of the zebra are well reconstructed, while the black areas are underexposed and not encoded by the patterns. Conversely, Figure 8 (middle) shows the reconstructions at a higher exposure time, which allows the reconstruction of the black areas, but overexposes the white regions. Finally, Figure 8 (right) shows the result of ITSL. Already one iteration can solve the problem caused by the color contrasts and allows the reconstruction of the entire surface. Fur-

ther iterations improve the quality slightly, but they should again be weighed according to the benefit and the recording time spent.

5.2.3 Specular Objects

As last and most important field of application of the method, we show its benefits in structured light reconstruction of specular objects. We apply the method to a specular metal sphere that strongly reflects the light emitted by the projector. The resulting highlighted areas are overexposed and cannot be encoded by the projected patterns. This effect cannot be completely avoided, but it can be greatly reduced. Figure 9 shows the reconstructed point clouds with standard structured light (left) and after one and two iterations of ITSL (center and right).

The highlighted points do not only depend on the projector's position relative to the object, but also on the camera perspective. To illustrate that the overexposed point is different for different camera positions, the point clouds in Figure 9 are triangulated from a pair of cameras instead of a camera-projector pair. Therefore, there are two independent faulty holes in the reconstructed point clouds from Figure 9. Finally, we would like to point out that this property means, that the defective area of the phase of one camera is most likely correctly encoded in the other camera. This can be used to improve reconstructions and to make them invariant to reflective objects in multiple camera structured light setups, as they are typical for practical applications.

6 CONCLUSION

In this paper, we have presented a method that greatly expands the practical scope of structured light reconstruction. Typical scenarios, in which the standard approach usually fails, are now treatable. Un-
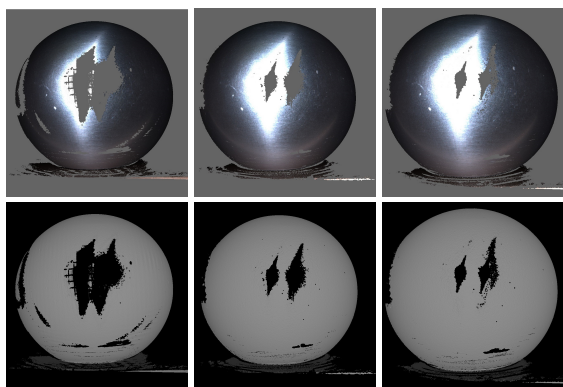
Figure 9: Triangulated point clouds of a specular sphere, captured from two views. Standard structured light (left) and results of ITSL after one and two iterations (middle and right). The top row shows the textured point clouds, while the bottom row visualizes the sole geometry.

favorably colored and reflective objects present no or significantly fewer problems. In the area of high-precision reconstruction, a significant leap in accuracy is achieved. However, the iterative character of the method also increases the recording time. Several iterations increase the accuracy, but should be weighed against the additional time required. Therefore, the approach is designed so that it can be easily built on existing setup and applied or omitted as needed.

REFERENCES

An, Y., Hyun, J.-S., and Zhang, S. (2016). Pixel-wise absolute phase unwrapping using geometric constraints of structured light system. *Optics express*, 24(16):18445–18459.

Bioucas-Dias, J. M. and Valadao, G. (2007). Phase unwrapping via graph cuts. *IEEE Transactions on Image processing*, 16(3):698–709.

Donlic, M., Petkovic, T., and Pribanic, T. (2015). 3d surface profilometry using phase shifting of de bruijn pattern. In *Proceedings of the IEEE International Conference on Computer Vision*, pages 963–971.

Fetzer, T., Reis, G., and Stricker, D. (2019). Robust auto-calibration for practical scanning setups from epipolar and trifocal relations. In *2019 16th International Conference on Machine Vision Applications (MVA)*, pages 1–6. IEEE.

Gupta, M., Yin, Q., and Nayar, S. K. (2013). Structured light in sunlight. In *Proceedings of the IEEE International Conference on Computer Vision*, pages 545–552.

Hartley, R. and Zisserman, A. (2003). *Multiple view geometry in computer vision*. Cambridge university press.

Lourakis, M. I. and Deriche, R. (2000). Camera self-calibration using the kruppa equations and the svd of the fundamental matrix: The case of varying intrinsic parameters.

Malacara, D. (2007). *Optical shop testing*. John Wiley & Sons.

Nayar, S. K., Krishnan, G., Grossberg, M. D., and Raskar, R. (2006). Fast separation of direct and global components of a scene using high frequency illumination. In *ACM Transactions on Graphics (TOG)*, volume 25, pages 935–944. ACM.

O'Toole, M., Mather, J., and Kutulakos, K. N. (2014). 3d shape and indirect appearance by structured light transport. In *Proceedings of the IEEE Conference on Computer Vision and Pattern Recognition*, pages 3246–3253.

O'Toole, M., Raskar, R., and Kutulakos, K. N. (2012). Primal-dual coding to probe light transport. *ACM Trans. Graph.*, 31(4):39–1.

Petković, T., Pribanić, T., and Đonlić, M. (2016). Single-shot dense 3d reconstruction using self-equalizing de bruijn sequence. *IEEE Transactions on Image Processing*, 25(11):5131–5144.

Sansoni, G. and Redaelli, E. (2005). A 3d vision system based on one-shot projection and phase demodulation for fast profilometry. *Measurement Science and Technology*, 16(5):1109.

Weinmann, M., Schwartz, C., Ruiters, R., and Klein, R. (2011). A multi-camera, multi-projector super-resolution framework for structured light. In *2011 International Conference on 3D Imaging, Modeling, Processing, Visualization and Transmission*, pages 397–404. IEEE.

Yang, L., Li, F., Xiong, Z., Shi, G., Niu, Y., and Li, R. (2017). Single-shot dense depth sensing with frequency-division multiplexing fringe projection. *Journal of Visual Communication and Image Representation*, 46:139–149.

Zhang, L., Curless, B., and Seitz, S. M. (2002). Rapid shape acquisition using color structured light and multi-pass dynamic programming. In *Proceedings. First International Symposium on 3D Data Processing Visualization and Transmission*, pages 24–36. IEEE.

Zhang, S. and Huang, P. (2004). High-resolution, real-time 3d shape acquisition. In *2004 Conference on Computer Vision and Pattern Recognition Workshop*, pages 28–28. IEEE.

Zhang, S. and Huang, P. S. (2006). High-resolution, real-time three-dimensional shape measurement. *Optical Engineering*, 45(12):123601.

Zhang, S. and Yau, S.-T. (2008). Three-dimensional shape measurement using a structured light system with dual cameras. *Optical Engineering*, 47(1):013604.

Zhang, Z. (1998). Determining the epipolar geometry and its uncertainty: A review. *International journal of computer vision*, 27(2):161–195.